# Chapter 14
# Diesel Engine SCR Systems: Modeling, Measurements, and Control

**Ming-Feng Hsieh and Junmin Wang**

## 14.1 Introduction

Selective catalytic reduction (SCR) systems have been successfully employed in industries for many decades. In recent years, its application scope on mobile vehicles has been significantly expanded due to the increasingly stringent emission regulations on Diesel engine powered vehicles worldwide. Comparing to the stationary applications (e.g., $NO_x$ reduction for power generation systems), mobile vehicle SCR systems present significant control challenges primarily due to the highly transient vehicle engine operations and thus the unpredictable engine-out emissions. Estimation and control of mobile vehicle SCR systems are the foci of this chapter.

Practical challenges on vehicle SCR system control mainly arise from the following aspects. First of all, the dynamics of many chemical reactions occurring within a urea-SCR together with the engine-out emissions and environmental variations create a nonlinear and complex plant for SCR urea dosing controller designs. In addition, many of the critical states within the SCR catalysts are hard to be directly measured on mobile vehicles due to the accessibility and cost constraints. For example, the amount of ammonia adsorbed by a catalyst, i.e., the $NO_x$ reduction reductant, is difficult to be directly measured. Moreover, current vehicle $NO_x$ sensors are cross-sensitive to ammonia, which causes issues on the tailpipe $NO_x$ measurement. The inaccurate $NO_x$ measurement not only affects the urea injection control but also the onboard diagnostics (OBD) which has been required by governmental regulations. Ammonia sensors are possible to be utilized as alternatives for providing feedback signals. But OBD systems need to correct the

M.-F. Hsieh
Cummins Inc., Columbus, IN 47201, USA

J. Wang (✉)
Department of Mechanical and Aerospace Engineering, The Ohio State University, Columbus, OH 43210, USA
e-mail: wang.1381@osu.edu

I. Nova and E. Tronconi (eds.), *Urea-SCR Technology for deNOx After Treatment of Diesel Exhausts*, Fundamental and Applied Catalysis,
DOI: 10.1007/978-1-4899-8071-7_14, 

tailpipe $NO_x$ concentration measurement to ensure the performance and emission reduction of the aftertreatment systems. Due to these aforementioned practical issues, systematic model-based SCR urea dosing control has been a great challenge. In this chapter, SCR control-oriented modeling is introduced in the first section to explain the basic system dynamics and characteristics. After that, some sensing and estimating systems for SCR catalysts are presented. Difficulties of current sensing systems and possible solutions are explained. At the end, SCR catalyst control systems and methods are discussed. An SCR ammonia storage distribution control method that can effectively reduce the SCR-outlet $NO_x$ and $NH_3$ emissions is introduced.

## 14.2 SCR Control-Oriented Modeling

### *14.2.1 Introduction*

While the dynamics of chemical reactions occurring within an SCR catalyst are quite complex, lumped-parameter 0-D mathematic models that can describe the essential SCR dynamics are preferred and often necessary for systematic real-time estimation and control system design purposes. The main challenge associated with the SCR catalyst control-oriented model development is to describe the SCR dynamics in a mathematically tractable way grounded in the in-depth understanding of the chemical reactions. Several studies that focused on the discoveries of fundamental SCR reactions using laboratory setups have been reported [1–9]. These studies offer insightful understandings to the chemical reaction mechanisms and the spatiotemporal distributions of species concentrations and temperature within the SCR catalysts. Accurately modeling the chemical reactions and fluid dynamics inside a catalyst requires the use of partial differential equations, which are computationally expensive and hard to be employed for real-time controller designs. Model reduction and valid assumptions need to be made in order to develop control-oriented SCR models. Several SCR models for the purposes of controller designs have be proposed recently, e.g., [10–13]. The following subsection introduces the basic approaches of developing SCR control-oriented models and the main assumptions made for such control-oriented models.

### *14.2.2 Main SCR Reactions*

The SCR $NO_x$ reduction process can be summarized by three major steps. In the first step, urea solution (AdBlue), as the source of the reductant ($NH_3$), is injected at the upstream of the catalyst and then is converted to $NH_3$. In the second step, the $NH_3$ inside the catalyst is adsorbed on the catalyst substrate. The adsorbed $NH_3$

can then catalytically react with $NO_x$ and convert them to nitrogen molecules and water, which is the third step. The key reactions of these processes are explained by the equations below:

*AdBlue (32.5 % aqueous urea solution (AdBlue)) evaporation*:

$$NH_2 - CO - NH_2(\text{liquid}) \rightarrow NH_2 - CO - NH_2^* + xH_2O, \tag{14.1}$$

*Urea decomposition*:

$$NH_2 - CO - NH_2^* \rightarrow NH_3 + HNCO, \tag{14.2}$$

*Isocyanic acid (HNCO) hydrolyzation*:

$$HNCO + H_2O \rightarrow NH_3 + CO_2. \tag{14.3}$$

*$NH_3$ Adsorption/Desorption*:

$$NH_3 + \theta_{\text{free}} \leftrightarrow NH_3^*, \tag{14.4}$$

*$NO_x$ Conversion*:

$$4NH_3^* + 4NO + O_2 \rightarrow 4N_2 + 6H_2O, \tag{14.5}$$

$$2NH_3^* + NO + NO_2 \rightarrow 2N_2 + 3H_2O, \tag{14.6}$$

$$4NH_3^* + 3NO_2 \rightarrow 3.5N_2 + 6H_2O. \tag{14.7}$$

*Ammonia Oxidation and NO Oxidation*:

$$4NH_3^* + 3O_2 \rightarrow 2N_2 + 6H_2O, \tag{14.8}$$

$$4NH_3^* + 5O_2 \rightarrow 4NO + 6H_2O, \tag{14.9}$$

$$4NH_3^* + 4O_2 \rightarrow 2N_2O + 6H_2O, \tag{14.10}$$

$$2NO + O_2 \rightarrow 2NO_2. \tag{14.11}$$

### 14.2.3 Control-Oriented SCR Model

The main reactions to be considered in the SCR control-oriented model are reactions of Eqs. (14.4), (14.5), (14.6), (14.8), and (14.11). Reactions which are ignored are the "slow SCR" in Eq. (14.7), ammonia oxidation to NO in Eq. (14.9), ammonia oxidation to $N_2O$ in Eq. (14.10), and the AdBlue to ammonia reactions of Eqs. (14.1), (14.2), and (14.3). Because the "fast SCR" is comparably much faster and most $NO_2$ can be converted by this process, the $NO_x$ after the upstream SCR catalyst is mostly NO. Consequently, the "slow SCR" in Eq. (14.7) is assumed to be a minor reaction. For ammonia oxidation, it has been reported that most of the SCR catalysts used on vehicles are 100 % selective toward $N_2$ [14],

and the oxidation reactions toward other species are all ignored. Besides, from the observations of ammonia measurements before the upstream SCR catalyst in [11]; it is believed that AdBlue can be completely converted to ammonia at the very upstream part of the SCR if the catalyst is well designed as well as the temperature and gas space velocity are sufficiently high. The AdBlue to ammonia conversion is thus assumed to be 100 % before entering the SCR catalyst.

The reaction rates of the processes being considered are modeled by Arrhenius equations. The reaction rate models are presented below:

$$4NH_3^* + 4NO + O_2 \rightarrow 4N_2 + 6H_2O, \tag{14.12}$$

$$R_1 = K_1 e^{-\frac{E_1}{RT}} C_{NO} C_{O_2} \theta \Theta V^2, \tag{14.13}$$

$$2NH_3^* + NO + NO_2 \rightarrow 2N_2 + 3H_2O, \tag{14.14}$$

$$R_2 = K_2 e^{-\frac{E_2}{RT}} C_{NO} C_{NO_2} \theta \Theta V^2, \tag{14.15}$$

$$4NH_3^* + 3O_2 \rightarrow 2N_2 + 6H_2O, \tag{14.16}$$

$$R_3 = K_3 e^{-\frac{E_3}{RT}} C_{O_2} \theta \Theta V, \tag{14.17}$$

$$NH_3 + \theta_{free} \leftrightarrow NH_3^*, \tag{14.18}$$

$$\text{forward}: R_{4F} = K_{4F} e^{-\frac{E_{4F}}{RT}} C_{NH_3} (1-\theta) \Theta V, \tag{14.19}$$

$$\text{reverse}: R_{4R} = K_{4R} e^{-\frac{E_{4R}}{RT}} \theta \Theta, \tag{14.20}$$

$$2NO + O_2 \rightarrow 2NO_2. \tag{14.21}$$

$$R_5 = K_5 e^{-\frac{E_5}{RT}} C_{NO} C_{O_2} V^2, \tag{14.22}$$

where $R_i$ are the reaction rates (mole/sec/m$^3$), $T$ is temperature, $C_x$ represents mole concentration of species $x$ (mole/m$^3$), $E_i$ (joule) and $K_i$ (unit depends on the elements in the reaction rate Arrhenius model) are the activation energy and rate constant of Arrhenius reaction model, $V$ is the catalyst volume (m$^3$), $\delta$ is the ammonia desorption efficiency, and $\theta$ is the ammonia coverage ratio defined as $\theta = M_{NH_3^*}/\Theta$. $M_{NH_3^*}$ represents the mole number of ammonia adsorbed by the SCR catalyst and $\Theta$ is the ammonia storage capacity of the catalyst (mole), which varies with temperature [3, 15, 16] and is modeled by the following equation:

$$\Theta = S_1 e^{-S_2 T}, \tag{14.23}$$

where $S_1$ and $S_2$, are positive constants. Note that the ammonia storage capacity can be significantly changed in an aged SCR system. The storage parameters ($S_1$ and $S_2$) need to be updated to capture the effect of catalyst aging. Another approach is to use an estimator to estimate the ammonia storage capacity variation

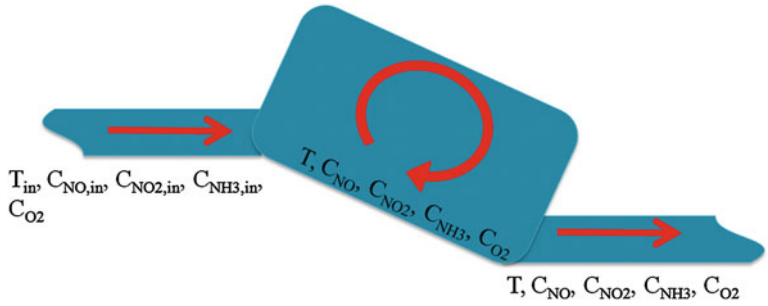


**Fig. 14.1** CSTR model of SCR catalyst [54]

and update the model intermittently. An ammonia storage variation estimation approach based on Extended Kalman Filter (EKF) is available in [17].

To avoid partial differential equations in the control-oriented model, the SCR catalyst is assumed to be a continuous stirred tank reactor (CSTR), as shown in Fig. 14.1, for developing a 0-D model [12]. Under this CSTR assumption, the states are considered homogenous within the catalyst. Based on the CSTR assumption and the mass conservation law, the dynamic equations of the considered states in a single SCR catalyst can be expressed below.

$$V\dot{C}_{\mathrm{NO}} = FC_{\mathrm{NO,in}} - R_1 - 0.5R_2 - R_5 - FC_{\mathrm{NO}}, \tag{14.24}$$

$$V\dot{C}_{\mathrm{NO_2}} = FC_{\mathrm{NO_2,in}} - 0.5R_2 - R_5 - FC_{\mathrm{NO_2}}, \tag{14.25}$$

$$V\dot{C}_{\mathrm{NH_3}} = FC_{\mathrm{NH_3,in}} - R_{4F} + R_{4R} - FC_{\mathrm{NH_3}}, \tag{14.26}$$

$$\dot{M}_{\mathrm{NH_3^*}} = R_{4F} - R_{4R} - R_1 - R_2 - R_3, \tag{14.27}$$

where $F$ is the exhaust flow rate into the catalyst, and it is assumed equal to the catalyst outlet flow rate, and $C_{x,\mathrm{in}}$ represent the species concentrations at the upstream of the catalyst. Practically, $C_{\mathrm{NO,in}}$ and $C_{\mathrm{NO_2,in}}$ cannot be directly measured because the current onboard $NO_x$ sensors cannot differentiate NO and $NO_2$ from $NO_x$. To address this problem, an observer needs to be designed to estimate $C_{\mathrm{NO,in}}$ and $C_{\mathrm{NO_2,in}}$. An example on how to design such an observer can be found in [18]. $C_{\mathrm{NH_3,in}}$, on the other hand, can be predicted by the AdBlue injection rate and is modeled by the following equation:

$$\dot{C}_{\mathrm{NH_3,in}} = -\alpha C_{\mathrm{NH_3,in}} + 2\alpha \frac{\tau u_{\mathrm{AdBlue}}}{N_{\mathrm{urea}} F}, \tag{14.28}$$

where $\alpha$ is a time-constant, $\tau$ is the mass fraction of urea in the AdBlue solution, $N_{\mathrm{urea}}$ is the atomic number of urea, and $u_{\mathrm{AdBlue}}$ is the mass injection rate of AdBlue upstream of the SCR system. The above SCR dynamic equations can then be rearranged into a state-space form as shown in Eq. (14.29).

$$\begin{bmatrix} \dot{C}_{NO} \\ \dot{C}_{NO_2} \\ \dot{C}_{NH_3} \\ \dot{\theta}_{NH_3} \\ \dot{C}_{NH_3,in} \end{bmatrix} = \begin{bmatrix} -r_1 C_{NO} C_{O_2} \theta_{NH_3} \Theta V - \frac{1}{2} r_2 C_{NO} C_{NO_2} \theta_{NH_3} \Theta V - r_5 C_{NO} C_{O_2} V - \frac{F}{V} C_{NO} + \frac{F}{V} C_{NO,in} \\ -\frac{1}{2} r_2 C_{NO} C_{NO_2} \theta_{NH_3} \Theta V + r_5 C_{NO} C_{O_2} V - \frac{F}{V} C_{NO_2} + \frac{F}{V} C_{NO_2,in} \\ -C_{NH_3} \left[ \Theta r_{4F} (1 - \theta_{NH_3}) + \frac{F}{V} \right] + \frac{1}{V} r_{4R} \Theta \theta_{NH_3} + \frac{F}{V} C_{NH_3,in} \\ -\theta_{NH_3} (r_{4F} C_{NH_3} V + r_3 C_{O_2} V + r_{4R} + r_1 C_{NO} C_{O_2} V^2 + r_2 C_{NO} C_{NO_2} V^2) + r_{4F} C_{NH_3} V \\ -\alpha C_{NH_3,in} + 2\alpha C_{AdBlue,inj} \end{bmatrix}, \tag{14.29}$$

$$r_i = K_i e^{-\frac{E_i}{RT}}, i = 1, 2, 3, 4F, 4R, 5. \tag{14.30}$$

Parameters of the model are strenuous to be calibrated due to the high number of parameters and the complexity of the chemical reactions. One way to calibrate the model effectively is to use the Genetic Algorithm (GA) to optimize the model parameters such that the model predictions best match with the calibration measurement data. GA has been known of optimizing complex and nonconvex equations. This feature makes it a good candidate to calibrate the SCR model. Detailed explanation of how to use GA to calibration the model and a calibration example is available in [11].

Notice that the model in Eq. (14.29) is to capture the main dynamics of a nominal SCR system. This dynamics can change as catalyst ages, but the main structure of the model should remain the same. Parameters of the chemical reaction rates and catalyst ammonia storage in the model should be updated if an aged system is to be considered. Because different catalyst formulations can have very different aging behaviors, it is not easy to have a general model to simulate the catalyst aging effects. A straightforward approach of capturing the catalyst aging behaviors would be to recalibrate the model for an aged catalyst, and then interpolate the characteristics between a fresh and an aged system to describe the aging process.

## 14.3 SCR Sensing and Estimation Systems

According to the SCR control-oriented model shown in Eq. (14.29), the key states of an SCR catalyst are: SCR inlet $NO_{(x)}$ concentration, SCR inlet $NH_3$ concentration, exhaust flow rate, SCR catalyst temperature, SCR-outlet $NO_x$ concentration, SCR-outlet $NH_3$ concentration, and SCR catalyst ammonia coverage ratio. Current vehicle onboard sensors are capable of measuring gas flow rate, temperature, $NO_x$ concentration, and $NH_3$ concentration. However, the current production $NO_x$ sensors are cross-sensitive to $NH_3$, which make the accurate measurement of SCR-outlet $NO_x$ concentration difficult. Without the information of SCR-outlet $NO_x$ concentration, closed-loop SCR control is difficult, and so is the diagnostics of SCR $NO_x$ reduction capability. Moreover, the catalyst ammonia coverage ratio ($\theta_{NH_3}$) is also hard to be directly measured. Ammonia coverage ratio is an inherent state in the SCR catalyst which directly affects the catalytic reactions. This state is

important for SCR urea real-time dosing control applications since it couples the tailpipe $NO_x$ and $NH_3$ dynamics.

$NO_x$ sensor ammonia cross-sensitivity and SCR catalyst ammonia coverage ratio have been the main challenges of the SCR sensing systems. The rest of this subsection provides some insight into these two problems and introduces some current solutions.

### *14.3.1 $NO_x$ Sensor $NH_3$ Cross-Sensitivity*

Figures 14.2, 14.3, and 14.4 show the test results of the $NO_x$ sensor ammonia cross-sensitivity based on the SCR system depicted in Figs. 14.16 and 14.17. The measurements of the $NO_x$ sensor between the two SCR catalysts together with the readings of a Horiba gas analyzer, the ammonia sensor, and the thermocouple are located at the same region. Different engine operating conditions and AdBlue injection rates were examined. In Fig. 14.2, the engine speed and accelerator pedal position were maintained at 1700 RPM and 27 %, and AdBlue injection started at the twentieth second with 0.15 g/s injecting rate in constant until the eight hundredth second. In the test of Fig. 14.3, these values were set to 1000 RPM, 18 %, and 0.1 g/s, respectively. The test presented in Fig. 14.4 consists of transient speed and accelerator pedal position profiles as shown in Fig. 14.5, and the AdBlue injection rate was kept at 0.1 g/s.

Assuming the $NO_x$ sensor is only cross-sensitive to ammonia and the Horiba gas analyzer readings are the actual exhaust gas $NO_x$ concentrations, based on these data and the $NO_x$ sensor ammonia cross-sensitivity model in Eq. (14.31), it can be clearly observed that the cross-sensitivity $K_{cs}$ is different in these tests and also changes with time. By the preliminary examinations of the data, it can be seen that the cross-sensitivity in the test of Fig. 14.2 was about 2, and was decreased to 0.5 in the test of Fig. 14.3. Furthermore, the value in the test of Fig. 14.4 was changing with time. In the light of these observations, it can be concluded that the $NO_x$ sensor ammonia cross-sensitivity is dynamic and cannot be simply treated as a constant for estimating the actual $NO_x$ concentration in exhaust gas.

$$C_{NO_x,sen} = C^*_{NO_x} + K_{cs} C_{NH_3}, \tag{14.31}$$

#### 14.3.1.1 EKF Approach for $NO_x$ Sensor Reading Correction

The challenge of estimating the $NO_x$ sensor ammonia cross-sensitivity factor lies in the fact that a dynamic model is hard to be developed. For the SCR-out $NO_x$ concentration estimation, it is possible to employ an accurate SCR model with a $NO_x$ sensor upstream of the SCR catalyst and the amount of AdBlue injection. However, such prediction requires a high-accuracy SCR model, which is

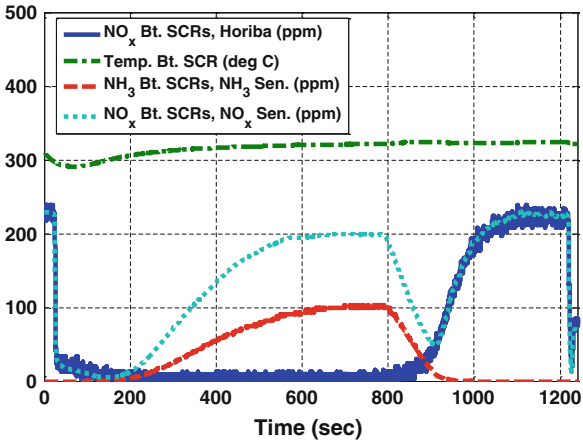


**Fig. 14.2** Engine speed 1700 RPM, accelerator pedal 27 %, AdBlue injection 0.15 g/s between 20 and 800 s [26]

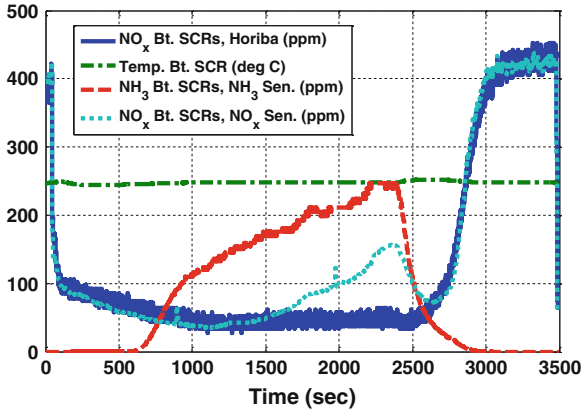


**Fig. 14.3** Engine speed 1000 RPM, gas pedal 18 %, AdBlue injection 0.1 g/s between 20 and 2400 s [26]

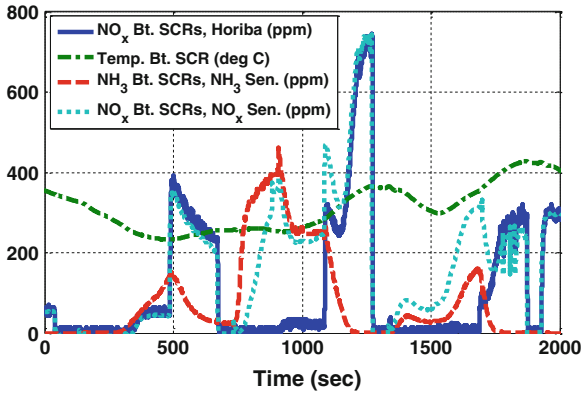


**Fig. 14.4** Transient test, AdBlue injection 0.15 g/s [26]

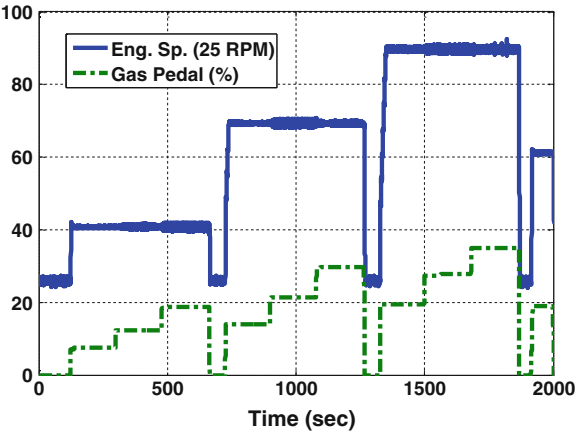


**Fig. 14.5** Engine speed and accelerator pedal profiles of the test in Fig. 4 [26]

challenging to be implemented on a mobile vehicle onboard controller because of the limited computational capability. To address the above problems, a possible solution is to use an extended Kalman filter (EKF) to estimate the $NO_x$ sensor ammonia cross-sensitivity factor and the actual $NO_x$ concentration at the same time [19].

Kalman filter is well known as an efficient recursive filter that can optimally estimate the states of linear dynamic systems from a series of noisy measurements [20]. For nonlinear systems, extended Kalman filters [21, 22] have been developed and validated by many studies to be effective in real applications [17, 23–25]. Unlike model-based estimators which heavily rely upon the plant models, a specific feature of a Kalman filter is that it finds the stochastic relations between model predictions and sensor measurements, and then estimates system states in an optimal approach. By utilizing this feature of the Kalman filter, a slowly time-varying state can be treated as a constant and its variation can be estimated by comparing the model predictions and measurements in a stochastic manner.

#### 14.3.1.2 EKF for Cross-Sensitivity Factor and $NO_x$ Concentration Estimations

According to the studies in [11] and [26], the cross-sensitivity factor $K_{cs}$ variation is mainly caused by temperature change. Because engine exhaust temperature dynamics after the SCR catalyst is generally slow, the cross-sensitivity factor $K_{cs}$ in Eq. (14.31) is assumed to be a slowly time-varying variable, and it can be modeled by the following equation:

$$\dot{K}_{cs} = 0. \tag{14.32}$$

Based on the SCR model in Eq. (14.29), the $NO_x$ concentration is modeled by the following equation:

$$\dot{C}^*_{NO} = -r_1 C^*_{NO} C_{O_2} \theta_{NH_3} \Theta V - \frac{1}{2} r_2 C^*_{NO} C^*_{NO_2} \theta_{NH_3} \Theta V - r_5 C^*_{NO} C_{O_2} V - \frac{F}{V} C^*_{NO} + \frac{F}{V} C_{NO,in}, \tag{14.33}$$

$$\dot{C}^*_{NO_2} = -\frac{1}{2} r_2 C^*_{NO} C^*_{NO_2} \theta_{NH_3} \Theta V + r_5 C^*_{NO} C_{O_2} V - \frac{F}{V} C^*_{NO_2} + \frac{F}{V} C_{NO_2,in}, \tag{14.34}$$

$$C^*_{NO_x} = C^*_{NO} + C^*_{NO_2}, \tag{14.35}$$

where $C_{NO,in}$ and $C_{NO_2,in}$ are estimated by an observer using the $NO_x$ sensor upstream of the SCR catalyst as described in [18, 27–29]. Since the $NO_x$ sensor used for $C_{NO,in}$ and $C_{NO_2,in}$ estimations is located upstream of the AdBlue injector, it is not affected by the ammonia cross-sensitivity and it can be assumed that $C_{NO,in} = C^*_{NO,in}$ and $C_{NO_2,in} = C^*_{NO_2,in}$. Here $\theta_{NH_3}$ is the SCR ammonia surface coverage ratio which can be estimated by the observer presented in the next section.

By the above models, the prediction equation in a discrete form is obtained as

$$x(k|k-1) = \begin{bmatrix} \hat{K}_{cs}(k|k-1) \\ \hat{C}^*_{NO}(k|k-1) \\ \hat{C}^*_{NO_2}(k|k-1) \end{bmatrix} = \begin{bmatrix} \hat{K}_{cs}(k-1|k-1) \\ \hat{C}^*_{NO}(k-1|k-1) + \Delta t \dot{\hat{C}}^*_{NO}(k-1|k-1) \\ \hat{C}^*_{NO_2}(k-1|k-1) + \Delta t \dot{\hat{C}}^*_{NO_2}(k-1|k-1) \end{bmatrix}, \tag{14.36}$$

where $\Delta t$ is the EKF updating period. The EKF measurement is the $NO_x$ sensor reading between the two SCR catalysts, which can be described as:

$$z(k) = C_{NO_x,sen}(k) = \hat{C}^*_{NO}(k|k-1) + \hat{C}^*_{NO_2}(k|k-1) + \hat{K}_{cs}(k|k-1) C_{NH_3}(k), \tag{14.37}$$

where $C_{NH_3}$ is the ammonia concentration measured by the ammonia sensor between the two SCR catalysts and the reading is assumed to be accurate enough.

Based on the prediction and measurement equations of Eqs. (14.36) and (14.37), the extended Kalman filter for the estimations of NO and $NO_2$ ($NO_x$) concentrations and the sensor ammonia cross-sensitivity factor can be constructed.

#### 14.3.1.3 Experimental Validations of the EKF

Figures 14.6, 14.7, 14.8, and 14.9 show the experimental results of the EKF estimations together with the $NO_x$ concentrations predicted by the SCR model in Eq. (14.29) and measured by a $NO_x$ sensor and a Horiba gas analyzer. Because the $NO_2$ concentrations measured after the SCR catalyst are always very low due to

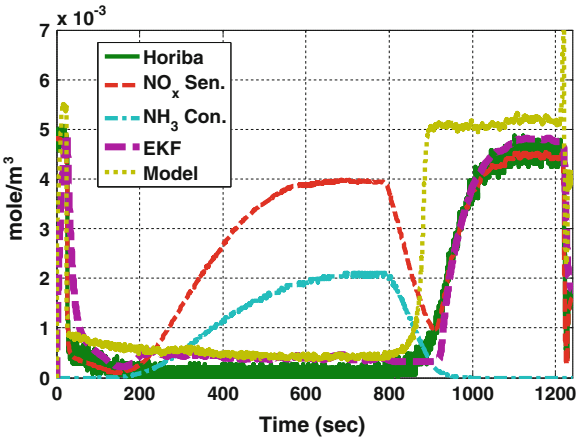


**Fig. 14.6** Comparison $NO_x$ concentration estimated by EKF, predicted by SCR model, measured by $NO_x$ sensor, and measured by Horiba gas analyzer in the test same as Fig. 2 [26]

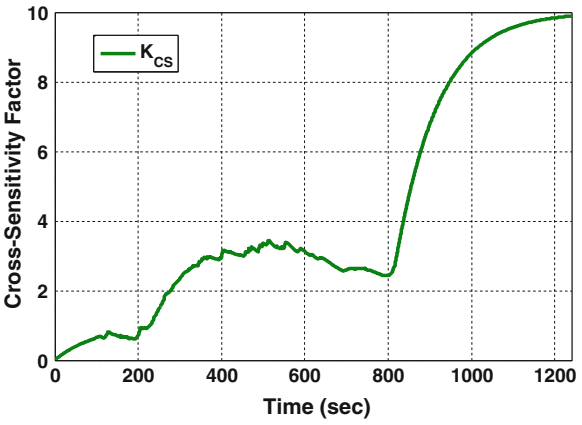


**Fig. 14.7** EKF estimated ammonia cross-sensitivity of the $NO_x$ sensor in the test of Fig. 6 [26]

the high reaction rate of the "fast SCR reaction" in Eq. (14.6), separate NO and $NO_2$ estimations are not addressed in this section, instead, the lumped $NO_x$ concentration is used.

From Figs. 14.6 and 14.8, it can be observed that by using the SCR model in Eq. (14.29) to predict the $NO_x$ concentration, i.e., without using the $NO_x$ sensor after SCR, the predicted value can be insensitive to the presence of ammonia. However, due to the uncertainties between the real plant and the simplified model, noticeable differences can be seen especially during transient periods. On the other hand, when the EKF was used to estimate the $NO_x$ concentration, the $NO_x$ EKF estimation results were considerably improved and they are very close to the Horiba gas analyzer measured $NO_x$ concentrations, which are assumed to be the actual values.

Figures 14.7 and 14.9 show the estimated $NO_x$ sensor ammonia cross-sensitivity of the tests been examined. It can be seen that, when ammonia slip was present to the $NO_x$ sensor, cross-sensitivity variations in each test can be correctly captured.

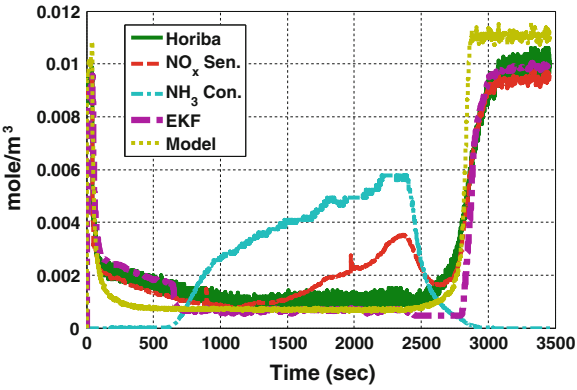


**Fig. 14.8** Comparison $NO_x$ concentration estimated by EKF, predicted by SCR model, measured by $NO_x$ sensor, and measured by Horiba gas analyzer in the test same as Fig. 3 [26]

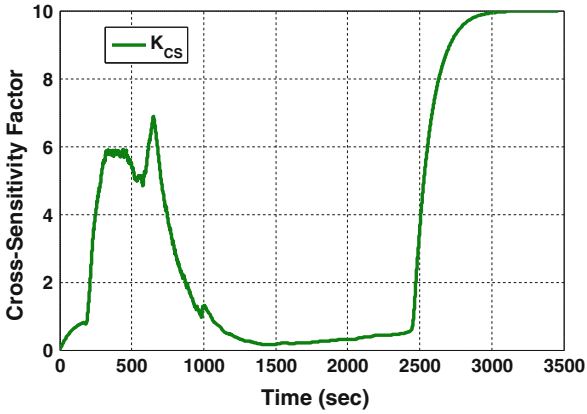


**Fig. 14.9** EKF estimated ammonia cross-sensitivity of the $NO_x$ sensor in the test of Fig. 14.8 [26]

During some time periods the ammonia cross-sensitivity estimations were raised to higher ranges, e.g., at the end of each test and between the 200–1,000 s in Fig. 14.9. These are because the ammonia slip was close to zero (lack of persistence of excitation) such that a higher cross-sensitivity was required to explain the difference between the $NO_x$ concentrations predicted by the model and sensor measurements. When ammonia is presented, the estimated cross-sensitivity converged back to the reasonable value as can be seen at around the thousandth second in Fig. 14.9. This cross-sensitivity error would not have a significant effect to the $NO_x$ concentration estimation since the ammonia emissions in these ranges were very low and the influence of cross-sensitivity was very limited. By setting a saturation to constrain the estimated cross-sensitivity value in a reasonable range (0–10 in the tests), undesired divergence can be avoided and the settling time to the actual cross-sensitivity, when ammonia slip is presented, can be reduced. On the other hand, even though the cross-sensitivity value is not directly useful for control applications, it has the potential to be used to diagnose the malfunction or aging effects of $NO_x$ and $NH_3$ sensors by checking the estimated value to be within a reasonable range which can change with temperature variations.

It is also important to note that the EKF estimation can lump model uncertainties into the slow variation term $K_{cs}$. So the variation term can contain more uncertainties if the EKF model is not accurate. This should be kept in mind if $K_{cs}$ is further to be used for diagnostics purpose.

## *14.3.2 SCR Catalyst Ammonia Coverage Ratio Estimation*

SCR catalyst ammonia coverage ratio is a critical state that affects the SCR system dynamics as well as the $NO_x$ conversion and tailpipe ammonia slip [30–33]. However, it is generally difficult to measure this signal onboard, even though some lab-based measurement methods have been proposed [34]. To perform appropriate real-time urea dosing control, it is thus beneficial to design an observer to estimate the SCR ammonia coverage ratio in real-time. In this subsection, two different nonlinear observers are designed based on the developed nonlinear SCR model (Eq. 14.29). The first observer is designed based on the ammonia coverage ratio dynamics. The sensitivity analysis of the observer shows that the observer is sustainable of small $NO_x$ and ammonia measurement errors, but is very sensitive to temperature measurement uncertainty. Besides, since the $NO_x$ sensor cross-sensitivity might not be completely compensated by the EKF correction approach at some points, e.g., before cross-sensitivity factor converges, the second observer is designed to be robust with respect to the temperature measurement errors and the $NO_x$ sensor uncertainty. In this observer, in addition to the ammonia coverage ratio dynamics, the ammonia concentration dynamics is also considered in the observer design, and a sliding mode approach was employed to increase the observer robustness with respect to the specific measurement errors and uncertainties. The sensitivity analyses of the observers are conducted and the effectiveness of the observers is verified by simulations with a vehicle model through the FTP75 test cycle.

### 14.3.2.1 Observer 1: Design Based on Coverage Ratio Dynamics

The first observer design is based on the $NH_3$ coverage ratio dynamics as shown in the SCR model of Eq. (14.29):

$$\begin{aligned}\dot{\theta}_{NH_3} = &- \theta_{NH_3}\left(r_{4F}C_{NH_3}V + r_3 C_{O_2}V + r_{4R} + r_1 C_{NO}C_{O_2}V^2 + r_2 C_{NO}C_{NO_2}V^2\right)\\ &+ r_{4F}C_{NH_3}V. \end{aligned} \tag{14.38}$$

From the SCR model, it can be seen that all the states and parameters but the ammonia coverage ratio $\theta_{NH_3}$ are available. Besides, since the $NO_2$ concentration after the SCR catalyst ($C_{NO_2}$) is always low, it can be assumed that $C_{NO_2} = 0$. Under this assumption, an observer can be designed in a straightforward manner.

With the above assumptions, the following observer can ensure the convergence of the estimation error.

$$\begin{aligned}\dot{\hat{\theta}}_{\mathrm{NH_3}} &= -\left(r_{4F}C_{\mathrm{NH_3}}V + r_3C_{\mathrm{O_2}}V + r_{4R} + r_1C_{\mathrm{NO}}C_{\mathrm{O_2}}V^2\right)\hat{\theta}_{\mathrm{NH_3}} + r_{4F}C_{\mathrm{NH_3}}V \\ &= -M_1\hat{\theta}_{\mathrm{NH_3}} + M_2, \hat{\theta}_{\mathrm{NH_3}} \le 1,\end{aligned} \tag{14.39}$$

where $M_1$ and $M_2$ are positive. The stability of this observer can be proved based on the Lyapunov theory, details of the stability proof can be found in [35, 36].

#### 14.3.2.2 Observer 2: Design Based on Coverage Ratio and $NH_3$ Dynamics

To reduce the estimation error caused by the temperature measurement and parametric uncertainties, a robust observer using the sliding mode technique by considering the $NH_3$ dynamics is designed. As the ammonia sensor is not cross-sensitive against $NO_x$, such a feature can be beneficial for the observer design. Also, based on the sensitivity analysis of the observer, the observer is robust to $NO_x$ sensor uncertainty, which is preferable especially when the $NO_x$ sensor cross-sensitivity is not completely compensated by the EKF correction approach.

Sliding mode observer is known for its robustness with respect to bounded uncertainties [37–41]. The observer considering the dynamics of ammonia coverage ratio and ammonia reaction is proposed as follows: The estimation error $\tilde{\theta}_{\mathrm{NH_3}}$ of the following observer will converge to zero in a finite period of time.

$$\dot{\hat{\theta}}_{\mathrm{NH_3}} = -\hat{\theta}_{\mathrm{NH_3}}\left(r'_{4F}C_{\mathrm{NH_3}}V + r'_3C_{\mathrm{O_2}}V + r'_{4R}\right) + r'_{4F}C_{\mathrm{NH_3}}V + K_\theta \mathrm{sign}(C_{\mathrm{NH_3}} - \hat{C}_{\mathrm{NH_3}}), \tag{14.40}$$

where

$$\begin{aligned}\dot{\hat{C}}_{NH_3} = &-C_{\mathrm{NH_3}}\left[\Theta r'_{4F}\left(1 - \hat{\theta}_{\mathrm{NH_3},2}\right) + \frac{F}{V}\right] + \frac{1}{V}r'_{4R}\Theta\hat{\theta}_{\mathrm{NH_3}} + \frac{F}{V}C_{\mathrm{NH_3,in}} \\ &+ K_{\mathrm{NH_3}}\mathrm{sign}\left(C_{\mathrm{NH_3}} - \hat{C}_{\mathrm{NH_3}}\right).\end{aligned} \tag{14.41}$$

The stability of this observer can also be proved based on the Lyapunov theory as detailed in [35, 36].

#### 14.3.2.3 Simulation Validations and Analyses

Simulated sensor errors were applied to the system to evaluate the observer sensitivities with respect to the measurement uncertainties. In this section, $NO_x$ sensor ammonia cross-sensitivity factor is modeled as a slow time-varying signal. If not specified, $NO_x$ sensor is subjected to a cross-sensitivity to ammonia as modeled in

**Table 14.1** Simulation cases with corresponding observers and sensor measurement variances

| Case | Observers | $NH_3$ Measurement variances | $NO_x$ Measurement Variances | T Measurement Variances | $K_x$ Variances | $NH_3$ Storage capacity variation |
|---|---|---|---|---|---|---|
| 1 | 1 | 1 | 1 | 1 | 1 | 1 |
| 2 | 1 | 1.5 | 1 | 1 | 1 | 1 |
| 3 | 1 | 1 | 1.8 | 1 | 1 | 1 |
| 4 | 1 | 1 | 1 | 1.1 | 1 | 1 |
| 5 | 2 | 1 | 1.8 | 1 | 1 | 1 |
| 6 | 2 | 1 | 1 | 1.1 | 1 | 1 |
| 7 | 2 | 1 | 0 | 1 | 1 | 1 |
| 8 | 2 | 1 | 1 | 1 | 1.5 | 1 |
| 9 | 2 | 1 | 1 | 1 | 1 | 1.5 |

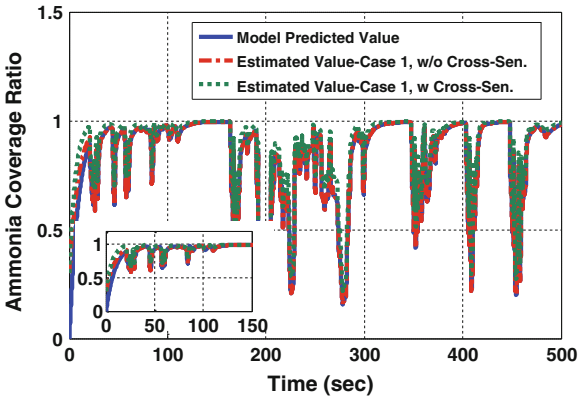


**Fig. 14.10** Performance of the observer 1 based on ammonia coverage ratio dynamics [35]

Eq. (14.31) and the cross-sensitivity is eliminated by the EKF. Nine cases were compared as listed in Table 14.1. The variances represent the sensor errors (i.e., 1 means there is no sensor error, 1.1 means the measured value is 1.1 times the actual value, and 0 means there is no measurement available and the measurement is 0). The $K_x$ is the pre-exponential factors of the considered SCR reactions. Also the ammonia storage capacity uncertainties are considered in observer 2. The initial $NH_3$ coverage ratio was set to 0.3 in the observers while the real value starts from 0.

Three signals compared in Fig. 14.10 are the actual ammonia coverage ratio predicted by the model, coverage ratio estimated by observer 1 in Eq. (14.39) subjected to a $NO_x$ sensor without cross-sensitivity, and coverage ratio estimated by observer 1 subjected to a $NO_x$ sensor with cross-sensitivity and the EKF correction. As can be seen in both cases, the estimated signals converged to and tracked the actual values fairly well. Comparing the cases where the $NO_x$ sensor

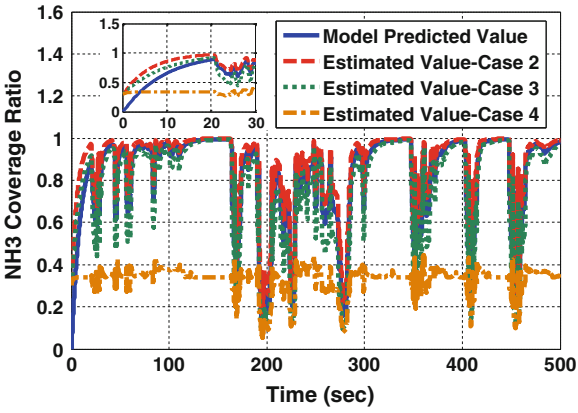


**Fig. 14.11** Observer 1 based on ammonia coverage ratio dynamics with sensor error [35]

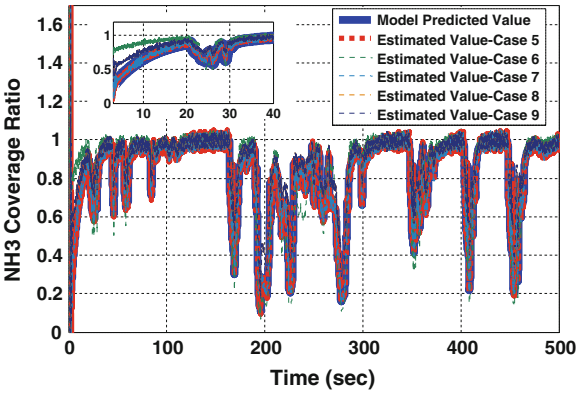


**Fig. 14.12** Observer 2 based on ammonia coverage ratio dynamics and ammonia dynamics [35]

does not have a cross-sensitivity and the one with a cross-sensitivity but subjected to the EKF correction, it can be observed that the difference between them can be hardly identified. This also verifies the applicability of the EKF for $NO_x$ sensor cross-sensitivity elimination.

Figure 14.11 shows the results when sensor errors were introduced to the observer. It can be seen that the NO and $NH_3$ sensor errors did not introduce significant influences to the estimations. However, a small offset of the temperature measurement caused an obvious difference between the real value and the estimated one. The same result (high sensitivity to temperature error) can also be obtained from the analysis of the observer sensitivities as conducted in [36].

Figure 14.12 shows the simulation results using the second observer described by Eq. (14.40). The observer depends on the measurement of $NH_3$ concentration. As expected, the observer is now robust to the temperature and $NO_x$ measurement errors and also to the chemical reaction rate errors. Since the observer can be robust to the $NO_x$ sensor measurement error, the $NO_x$ sensor cross-sensitivity issue

will not cause a significant estimation error to the observer. It can be seen that the estimated value contains noticeable noise, which is due to the chattering effect at the sliding mode. As can be seen in Case 7, the observer can still estimate the signal very accurately even without the $NO_x$ measurement. In Case 8, parametric uncertainties of the chemical reaction rates were imposed in a fashion such that the reduction rate constants of all considered chemical reactions were 1.5 times higher than the corresponding values in the model. Since the observer was designed to be robust to the reaction rates, the estimated ammonia coverage ratio still converged to the model value very well. Case 9 shows the situation when the SCR catalyst ammonia storage capacity is 1.5 times of the modeled value. As expected, the observer is also robust to this uncertainty.

## 14.4 SCR Control

Several SCR control designs for automotive and commercial vehicle applications have been proposed in recent years [10, 15, 30, 42–51]. Most of them focused on feed-forward controller designs or utilized linearized SCR models for feedback controller designs [10, 30, 45, 46, 48]. The study in [15] pointed out that open-loop feed-forward control cannot well handle the engine transient exhaust gas conditions and feedback control is necessary to compensate for the uncertainties during real-world driving as well as test cycles. To meet the recent stringent emission standards, some feedback controllers which utilize $NO_x$ sensors have been proposed [10, 30, 42, 45–47]. However, due to the $NO_x$ sensor ammonia cross-sensitivity and ammonia slip concerns, $NO_x$-based feedback control alone may be difficult to meet the SCR control objectives [15, 46, 47, 52]. Of late, with the availability of the automotive ammonia sensor from some suppliers such as Delphi, several $NH_3$-based feedback controls have been studied [49–51]. Such ammonia sensors may not be cross-sensitive to $NO_x$ or other major exhaust gas species, and is being considered by the industry as an alternative feedback sensor for urea-SCR system control. But because the sensor has not been in production yet, practical applications of ammonia sensor-based SCR control are rarely seen.

The objective of urea-SCR control is to simultaneously minimize the tailpipe $NO_x$ and ammonia emissions. Due to the nature of SCR dynamics, intuitively, increasing AdBlue injection rate can generally decrease SCR-out $NO_x$ emissions but also result in ammonia slip increases, and vice versa. To achieve low $NO_x$ and ammonia emissions simultaneously, specific control approaches need to be designed to handle the SCR nonlinear dynamics.

With an adequate amount of ammonia being adsorbed on the SCR substrate, high $NO_x$ reduction rate can be realized. It is thus believed that consistent SCR $NO_x$ reduction can be ensured by ammonia storage control. However, besides the $NO_x$ reduction, tailpipe ammonia slip constraint is another objective needs to be taken into account. From the SCR model in Eq. (14.29) and the ammonia adsorption/desorption reactions in Eq. (14.4), it can be seen that high ammonia

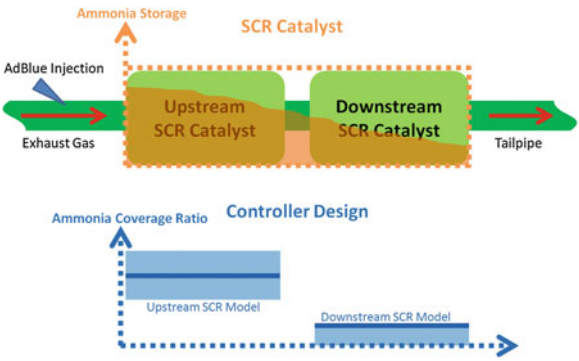


**Fig. 14.13** Schematic presentation of ammonia storage distribution control strategy [53]

coverage ratio/storage can directly lead to high SCR-out ammonia slip. Therefore, for low tailpipe ammonia slip, low ammonia coverage ratio/storage is desired, which contradicts to the intention of SCR $NO_x$ reduction (requires high ammonia coverage ratio).

To address the aforementioned contradiction, an ammonia storage distribution control (ASDC) approach is proposed. A schematic presentation of the ASDC concept is shown in Fig. 14.13. The control approach is to simultaneously achieve $NO_x$ and ammonia slip reductions by regulating the ammonia storage distribution along the axial direction of the SCR catalyst. The urea injection control objectives are: (1) to have rich ammonia storage at the upstream part of the SCR catalyst for accomplishing sufficient and efficient $NO_x$ reduction; and (2) to have lean ammonia storage at the downstream part such that the ammonia slip from the ammonia rich region (upstream) can be adsorbed and the tailpipe ammonia slip due to ammonia desorption from the downstream catalyst is limited. By this control approach, the SCR catalyst can be fully utilized such that the SCR $NO_x$ reduction and AdBlue utilization efficiencies can be enhanced while restricting the tailpipe ammonia slip.

To verify this ammonia storage distribution control approach in practice, a two-catalyst SCR system is developed. A controller is designed to control the AdBlue injection such that the ammonia coverage ratio of the upstream catalyst is kept at a higher value and the ammonia coverage ratio of the downstream catalyst is limited under a lower level as presented in Fig. 14.13.

### *14.4.1 Control-Oriented SCR Model*

The control-oriented SCR model proposed in Eq. (14.29) is extended to a two-cell model for the ASDC application as shown in Eq. (14.42), and a schematic presentation is shown in Fig. 14.14.

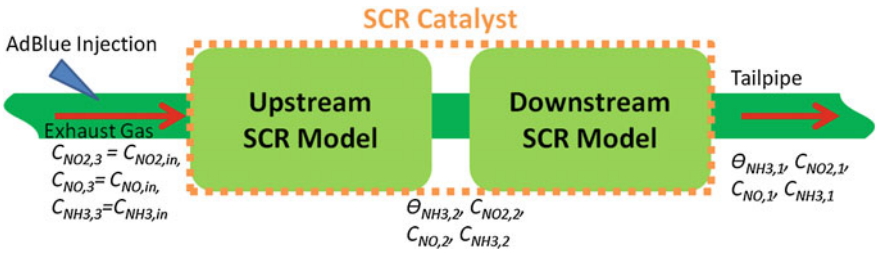


**Fig. 14.14** Schematic presentation of a two-cell SCR model [53]

$$\begin{bmatrix} \dot{C}_{\mathrm{NO},i} \\ \dot{C}_{\mathrm{NO}_2,i} \\ \dot{C}_{\mathrm{NH}_3,i} \\ \dot{\theta}_{\mathrm{NH}_3,i} \end{bmatrix} = \begin{bmatrix} -r_{1,i}C_{\mathrm{NO},i}C_{\mathrm{O}_2,i}\theta_{\mathrm{NH}_3,i}\Theta_i V_i - \frac{1}{2}r_{2,i}C_{\mathrm{NO},i}C_{\mathrm{NO}_2,i}\theta_{\mathrm{NH}_3,i}\Theta_i V_i - r_{5,i}C_{\mathrm{NO},i}C_{\mathrm{O}_2,i}V_i - \frac{F_i}{V_i}C_{\mathrm{NO},i} + \frac{F_i}{V_i}C_{\mathrm{NO},i+1} \\ -\frac{1}{2}r_{2,i}C_{\mathrm{NO},i}C_{\mathrm{NO}_2,i}\theta_{\mathrm{NH}_3,i}\Theta_i V_i - r_{5,i}C_{\mathrm{NO},i}C_{\mathrm{O}_2,i}V_i - \frac{F_i}{V_i}C_{\mathrm{NO},i} + \frac{F_i}{V_i}C_{\mathrm{NO},i+1} \\ -C_{\mathrm{NH}_3,i}\left[\Theta_i r_{4F,i}\left(1-\theta_{\mathrm{NH}_3,i}\right) + \frac{F_i}{V_i}\right] + \frac{1}{V_i}r_{4R,i}\Theta_i\theta_{\mathrm{NH}_3,i} + \frac{F_i}{V_i}C_{\mathrm{NH}_3,i+1} \\ -\theta_{\mathrm{NH}_3,i}\left(r_{4F,i}C_{\mathrm{NH}_3,i}V_i + r_{3,i}C_{\mathrm{O}_2,i}V_i + r_{4R,i} + r_{1,i}C_{\mathrm{NO},i}C_{\mathrm{O}_2,i}V_i^2 + r_{2,i}C_{\mathrm{NO},i}C_{\mathrm{NO}_2,i}V_i^2\right) + r_{4F,i}C_{\mathrm{NH}_3,i}V_i \end{bmatrix}$$

$i = 1, 2.$

(14.42)

Notice that because the catalyst volume of the above model is ½ of the complete SCR catalyst volume, the two-cell model not only can capture the state variations from upstream to downstream, but also has a better approximation to the CSTR assumption comparing to a single-cell model where the catalyst volume is twice larger. Besides, by the ammonia coverage ratio observers proposed in the last section and by assuming temperature, $NO_x$ concentration and ammonia concentration measurements are available at the downstream of the SCR catalysts and between the two catalysts; the model in Eq. (14.42) is full-state available.

### *14.4.2 Controller Design and Architecture*

In order to handle the complicated dynamics caused by the cascade connection of two SCR models, the backstepping control approach is used to design the controller. Also because the catalyst ammonia storage capacity has the highest uncertainty among other model variables [11], the controller is designed to be adaptive to the ammonia storage capacity. To regulate the ammonia coverage ratio of the upstream catalyst $\theta_{\mathrm{NH}_3,2}$ to a desired value $\theta^*_{\mathrm{NH}_3,2}$ while constraining the ammonia coverage ratio of the downstream catalyst $\theta_{\mathrm{NH}_3,1}$ under an upper limit of $\theta^*_{\mathrm{NH}_3,1}$, based on the control plant model, the urea dosing control law is proposed below:

$$C_{\mathrm{NH_3,in}} = -\frac{V_2}{F_2}\left\{G\left(\tilde{\theta}_{\mathrm{NH_3},1}\right)\left[\tilde{\theta}_{\mathrm{NH_3},2} r_{4F,2} V_2\left(1-\theta_{\mathrm{NH_3},2}\right) - \dot{\bar{C}}_{\mathrm{NH_3,2}} - \frac{F_2}{V_2} C_{\mathrm{NH_3,2}} - C_{\mathrm{NH_3,2}} r_{4F,2}\left(1-\theta_{\mathrm{NH_3},2}\right)\right] + \frac{1}{V_2} r_{4R,2}\theta_{\mathrm{NH_3,2}}\hat{\Theta}_2 + K_2\tilde{C}_{\mathrm{NH_3,2}}\left|\tilde{\theta}_{\mathrm{NH_3},2}\right|\right\}, \tag{14.43}$$

where,

$$\tilde{\theta}_{\mathrm{NH_3},1} = \theta_{\mathrm{NH_3},1} - \theta^*_{\mathrm{NH_3},1}, \tag{14.44}$$

$$\tilde{\theta}_{\mathrm{NH_3},2} = \theta_{\mathrm{NH_3},2} - \theta^*_{\mathrm{NH_3},2}, \tag{14.45}$$

$$\tilde{C}_{\mathrm{NH_3,2}} = C_{\mathrm{NH_3,2}} - \bar{C}_{\mathrm{NH_3,2}}, \tag{14.46}$$

$$\dot{\hat{\Theta}}_2 = \tilde{C}_{\mathrm{NH_3,2}}\left[C_{\mathrm{NH_3,2}} r_{4F,2}\left(1-\theta_{\mathrm{NH_3},2}\right) - \frac{1}{V_2} r_{4R,2}\theta_{\mathrm{NH_3,2}}\right], \tag{14.47}$$

$$\bar{C}_{\mathrm{NH_3,2}} = \frac{1}{r_{4F,2}V_2\left(1-\theta_{\mathrm{NH_3},2}\right)}\left[\theta_{\mathrm{NH_3},2}\left(r_{3,2}C_{\mathrm{O_2},2}V_2 + r_{4R,2} + r_{1,2}C_{\mathrm{NO},2}C_{\mathrm{O_2},2}V_2^2\right)G(\tilde{\theta}_{\mathrm{NH_3},1}) - K_1\tilde{\theta}_{\mathrm{NH_3},2}\right], \tag{14.48}$$

$$G(x) = \frac{1}{2}\mathrm{sign}(-x) + \frac{1}{2}, \mathrm{sign}(0) \equiv 0, \tag{14.49}$$

$K_1$, $K_2$, $K_3 > 0$.

The stability of the control law can be proved based on a backstepping analysis approach. Details of the stability proof process can be found in [53].

The complete SCR control architecture for practical applications is summarized in Fig. 14.15, which includes the SCR ammonia coverage ratio observer proposed in Eq. (14.40) (observer 2) and the EKF $NO_x$ sensor correction approach discussed previously.

### *14.4.3 Experimental Setup*

A schematic presentation and a picture of the experimental setup are shown in Figs. 14.16 and 14.17, respectively, which include: a medium-duty Diesel engine, Diesel oxidation catalyst (DOC)/Diesel particulate filter (DPF), and two SCR catalysts in series at downstream of the DOC/DPF. For the emission measurement system, a Horiba MEXA 7500 gas analyzer was used to measure the tailpipe $NO_x$ emissions. Three Siemens VDO (NGK) $NO_x$ sensors and two Delphi ammonia sensors were used to provide feedback information to the SCR controller and to monitor the emission levels at different locations as shown in Figs. 14.16 and 14.17.

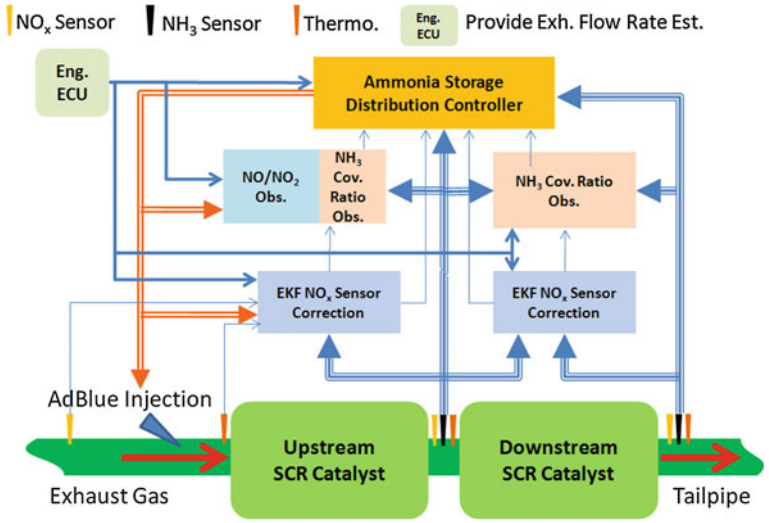


**Fig. 14.15** Schematic presentation of the controller architecture [53]

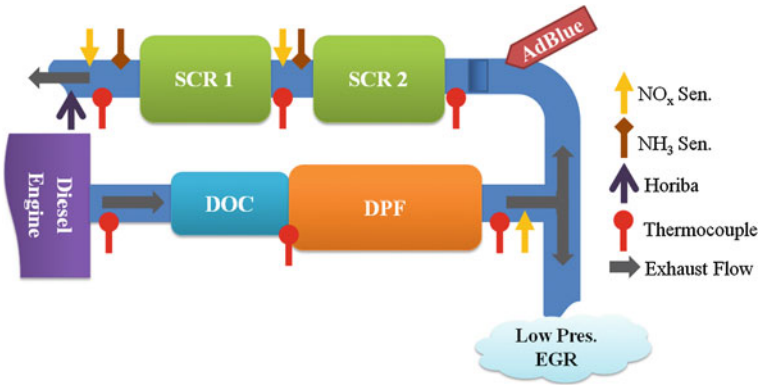


**Fig. 14.16** Schematic presentation of the experiment setup [53]

The $NO_x$ sensors were calibrated with a Horiba gas analyzer up to 1500 PPM and the ammonia sensors were calibrated with a FTIR up to 500 PPM. Notice that this experimental setup is to validate the concept of controlling ammonia storage distribution, and multiple $NO_x$ and $NH_3$ sensors are used. The number of sensors used for SCR control can be limited in real applications due to cost consideration.

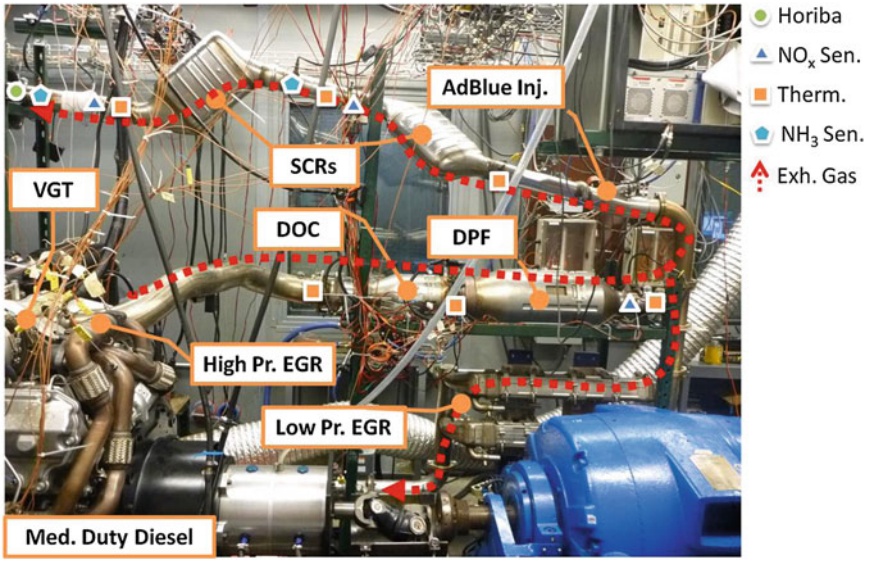


**Fig. 14.17** Diesel engine and aftertreatment system test bench [53]

### *14.4.4 Experimental Results of US06 Test Cycle*

Figure 14.18 shows the engine speed, torque, and SCR temperatures during the US06 test cycle conducted on a diesel engine motoring dynamometer setup. The ammonia coverage ratios of the two catalysts are shown in Fig. 14.19. The desired values of $\theta^*_{NH_3,1}$ and $\theta^*_{NH_3,2}$ were set to 0.3 and 0.6, respectively.

At the time around the four hundredth second, the downstream ammonia coverage ratio was increased and approached the upper limit (0.3). This increase was due to the temperature rise which induced an SCR ammonia storage capacity decrease. In this situation, as can be seen in Fig. 14.20, the controller reduced the AdBlue injection rate such that the downstream ammonia coverage ratio was restricted under the limit. In addition, as can be seen in Fig. 14.19, to satisfy the downstream catalyst ammonia coverage ratio constraint, lower upstream ammonia coverage ratio was inevitably accompanied. However, by comparing the ammonia coverage ratios of the two catalysts, the value of the upstream catalyst was always higher than that of the downstream catalyst, and the constraint of the ammonia coverage ratio for the downstream catalyst value was also satisfied. Thus, the main objectives of the ASDC were achieved.

Figure 14.20 illustrates the measured $NO_x$ and ammonia concentrations before, between, and after the SCR catalysts during the US06 test cycle. As can be observed, with the rich ammonia storage at the upstream catalyst, the engine exhaust $NO_x$ emissions were consistently reduced to low levels even if the engine-out $NO_x$ concentrations varied in a high frequency fashion. A zoom-in figure of the

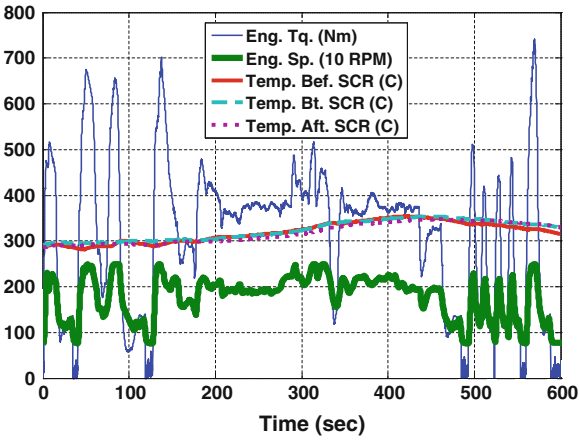


**Fig. 14.18** Engine operating condition and SCR catalyst temperatures in the US06 cycle test [53]

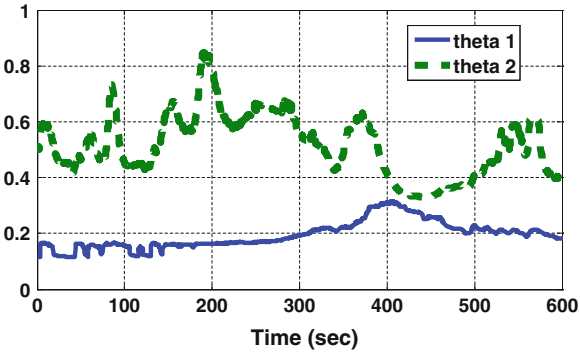


**Fig. 14.19** Ammonia coverage ratios of the two SCR catalysts in the US06 cycle test [53]

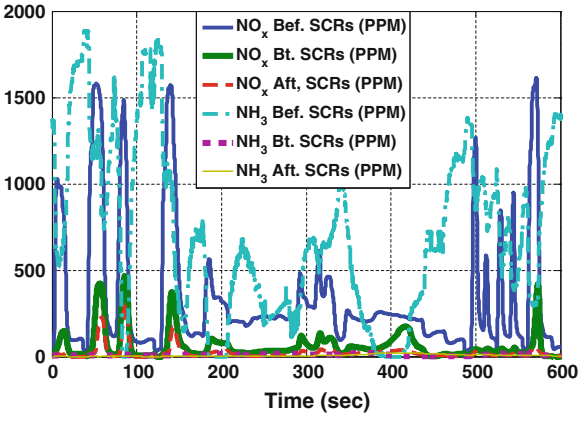


**Fig. 14.20** Measured $NO_x$ and $NH_3$ concentrations before, between, and after the SCR catalysts in the US06 cycle test [53]

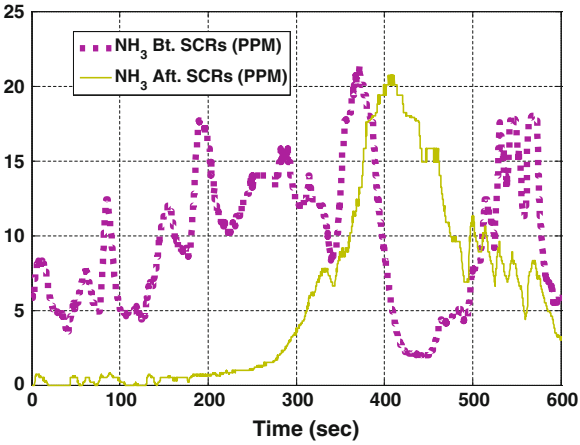


**Fig. 14.21** Measured ammonia slips between the two SCR catalysts and downstream of the SCR catalysts (tailpipe) in the US06 cycle test [53]

ammonia concentrations between and after the SCR catalyst is presented in Fig. 14.21. As it indicates, the higher ammonia slip from the upstream catalyst can be reduced by the downstream catalyst. At the time period between 400–500 s, higher ammonia slip was observed after the downstream SCR catalyst (i.e., at the tailpipe). This was primarily due to the ammonia storage capacity reduction caused by the increased catalyst temperature as mentioned before. The SCR ammonia storage capacity decrease induced a higher ammonia coverage ratio, which caused faster ammonia desorption rates and higher ammonia slip out of the downstream catalyst. As can be clearly observed from the ammonia concentration upstream of the SCR catalysts, the controller was able to reduce the AdBlue injection in this situation to avoid high ammonia slip from the catalysts. From the measurements, it can be seen that the tailpipe ammonia slip was reduced after it reached the maximum value of 20 ppm. The ammonia coverage ratios together with the tailpipe $NO_x$ and ammonia emissions resumed into the regular ranges after this transient temperature variation. More details about the experimental validations of the SCR ammonia storage distribution controller can be found in [53].

## 14.5 Conclusions

SCR control for mobile vehicle applications has been a great challenge in the aspects of estimation and controller designs. Some of the major issues, e.g., $NO_x$ sensor ammonia cross-sensitivity, SCR ammonia storage estimation, and SCR controller design, have been introduced in this chapter, and possible solutions are addressed. Most of the present solutions have been experimentally validated (except the observer for ammonia coverage ratio which currently cannot be directly measured). However, there are still some concerns which make robust and high $NO_x$ conversion efficiency SCR control challenging to be realized in

real-world vehicle driving. For example, costs of the emissions sensors (i.e., $NO_x$ and $NH_3$ sensors) and uncertainties from urea injection quantity, SCR formulation, and other measurements. Open problems on sensor reduction and development, as well as robustness of the control systems still need further research.

## References


1. Grossale A et al (2008) The chemistry of the $NO/NO_2$-$NH_3$ "fast" SCR reaction over Fe-$ZSM_5$ investigated by transient reaction analysis, *Journal of Catalysts*, 256:312–322
2. Nova I et al (2007) $NH_3$-$NO/NO_2$ SCR for Diesel exhausts aftertreatment: mechanism and modeling of a catalytic converter, *Topics in Catalysis*, 42:43–46
3. Ciardelli C et al (2004) SCR-$DeNO_x$ for diesel engine exhaust aftertreatment: unsteady-state kinetic study and monolith reactor modeling, *Chemical Engineering Science*, 59:5301–5309
4. Tronconi E et al (2005) Modeling of an SCR catalyst converter for diesel exhaust after treatment: dynamic effects at low temperature, *Catalysis Today*, 105:529–536
5. York A et al (2004) Modeling an ammonia SCR $DeNO_x$ catalyst: model development and validation, *Proceedings of the SAE 2004 World Congress*, SAE paper 2004-01-0155
6. Chatterjee D et al (2005) Numerical simulation of ammonia SCR-Catalytic converters: model development and application, *SAE 2005 World Congress*, SAE paper 2005-01-0965
7. Piazzesi G et al (2006) Isocyanic acid hydrolysis over Fe-$ZAM_5$ in urea SCR", *Catalysis Communications*, 7:600–602
8. Sluder CS et al (2004) Low temperature urea decomposition and SCR performance", *SAE 2004 World Congress*, SAE paper 05FL-55
9. Birkhold F et al (2007) Modeling and simulation of the injection of urea-water-solution for automotive SCR $DeNO_x$-systems, *Applied Catalysis B: Environmental*, 70:119–127
10. Schar CM et al (2004) Control-oriented model of an SCR catalytic converter system, *2004 SAE World Congress*, SAE paper 2004-01-0153
11. Hsieh M-F, Wang J (2011) Development and experimental studies of a control-oriented SCR model for a two-catalyst SCR system, *Control Engineering Practice*, 19(4):409–422
12. Upadhyay D, Van Nieuwstadt M (2002) Modeling of a urea SCR catalyst with automotive application, *Proceedings of the ASME International Mechanical Engineering Congress & Exposition*
13. Devarakonda M et al (2008) Adequacy of reduced order models for model-based control in a urea-SCR aftertreatment system, *SAE 2008 World Congress*, SAE paper 2008-01-0617
14. Devadas M, Krocher O, Wokaun A (2005) Catalytic investigation of $FeZSM_5$ in the selective catalytic reduction of $NO_x$ with $NH_3$, *Reaction Kinetics and Catalysis Letters*, 86:347–354
15. Willems F et al (2007) Is closed-loop SCR control required to meet future emission targets?, *SAE 2007 World Congress*, SAE paper 2007-01-1574
16. Joo K et al (2008) The study of $NO_x$ reduction using urea-SCR system with CPF and DOC for light Duty vehicle: the Diesel $NO_x$ reduction system, *2008 SAE World Congress*, SAE paper 2008-02-1183
17. Hsieh M-F, Wang J (2010) An extended Kalman filter for ammonia coverage ratio and capacity estimations in the application of Diesel engine SCR control and onboard diagnostics, *Proceedings of the 2010 American Control Conference*, 5875–5879
18. Hsieh M-F, Wang J (2011) NO and $NO_2$ Concentration Modeling and Observer-Based Estimation across a Diesel Engine Aftertreatment System, *ASME Transactions Journal of Dynamic Systems, Measurement, and Control*, 133(4):041005
19. Hsieh M-F, Wang J (2010) An extended Kalman filter for $NO_x$ sensor cross-sensitivity error elimination in Diesel engine selective catalytic application, *Proceedings of the 2010 American Control Conference*, 3033–3038

20. Kalman R (1960) A new approach to linear filtering and prediction problems, *ASME Journal of Basic Engineering*, 82(D):35–45
21. Julier SJ, Uhlmann JK (1997) A new extension of the Kalman filter to nonlinear system, *Proceedings of the Int. Symp. Aerospace/Defense Sensing, Simulation, and Control*
22. Wan EA, Van Der Merwe R (2000) The unscented Kalman filter for nonlinear estimation, *Proceedings of the IEEE 2000 Adaptive Systems for Signal Processing*: *Communication, and Control Symposium*, 153–158
23. Baumgartner ET, Skaar SB (1994) An autonomous vision-based mobile robot, *Proceedings of the IEEE Transaction on Automatic Control*, 39(3):493–502
24. Carlson HA et al (2006) A regulator and filter for tracking aerodynamic force", *Proceedings of the IEEE Conference on Decision and Control*, 4591–4596
25. Redmill K et al (2001) DGPS/INS integrated positioning for control of automated vehicle, *Proceedings of the 2001 IEEE Intelligence Transportation Systems Conference*
26. Hsieh M-F, Wang J (2011) Design and experimental validation of an extended Kalman filter-based $NO_x$ concentration estimator in selective catalytic reduction system applications, Control Engineering Practice, 19(4): 346–353.
27. Hsieh M-F, Wang J (2010) A physically-based, control-oriented diesel oxidation catalyst (DOC) model for the applications of $NO/NO_2$ ratio estimation using a $NO_x$ Sensor, *Proceedings of the ASME Dynamic Systems and Control Conference*
28. Hsieh M-F, Wang J (2010) A physically-based, control-oriented Diesel particulate filter (DPF) model for the applications of $NO/NO_2$ ratio estimation using a $NO_x$ sensor, *Proceedings of the ASME Dynamic Systems and Control Conference*
29. M. Hsieh and J. Wang, "Observer-based estimation of Diesel engine aftertreatment system NO and $NO_2$ concentrations", *Proceedings of the ASME Dynamic Systems and Control Conference,* (Invited Paper), 2010.
30. Upadhyay D, Van Nieuwstadt M (2006) Model based analysis and control design of a urea-SCR de$NO_x$ aftertreatment system, *ASME, Journal of Dynamic Systems, Measurement, and Control*, 128:737–741
31. Hsieh M-F, Wang J (2009) Backstepping based nonlinear ammonia surface coverage ratios control for diesel engine selective catalytic reduction systems, *Proceedings of the ASME Dynamic Systems and Control Conference*
32. Hsieh M-F, Wang J (2009) Diesel engine selective catalytic reduction ammonia surface coverage control using a computationally-efficient model predictive control assisted method, *Proceedings of the ASME Dynamic Systems and Control Conference*
33. Hsieh M-F, Wang J (2011) A two-cell backstepping based control strategy for Diesel engine selective catalytic reduction systems, *IEEE Transactions on Control Systems Technology*, 19(6):1504–1515
34. Kubinski DJ, Visser JH (2008), Sensor and method for determining the ammonia loading of a zeolite SCR catalyst, *Sensor and Actuator*, 130:425–429
35. Hsieh M-F, Wang J (2010) Observer-based estimation of selective catalytic reduction (SCR) catalyst ammonia storage *Journal of Automobile Engineering*, *Proceedings of the Institution of Mechanical Engineers Part D*, 224(9):1199–1211
36. Hsieh M-F, Wang J (2009) Nonlinear observer designs for Diesel engine selective catalytic reduction (SCR) ammonia coverage ratio estimation, Proceedings of the 48th IEEE Conference on Decision and Control, 6596–6601.
37. Drakunov SV (1992) Sliding-mode observers based on equivalent control method, *Proceedings of the 31th Conference on Decision and Control*, 2:2368–2369
38. Drakunov SV, Utkin V (1995) Sliding mode observers tutorial", *Proceedings of the 34th Conference on Decision and Control*, 4:3376–3378
39. Xiong Y, Saif M (2001) Sliding mode observer for nonlinear uncertain systems, *IEEE Transactions on Automatic Control*, 46(12):2012–2017
40. Utkin V et al (1999) Sliding mode control in electromechanical systems, *Taylor and Francis*
41. Slotine JJ et al (1987) On sliding observers for nonlinear systems," *ASME Journal of Dynamic Systems, Measurement, and Control*, 109:245–252

42. Song Q, Zhu G. (2002) Model-based closed-loop control of urea SCR exhaust aftertreatment system for Diesel engine, SAE 2002 World Congress, 2002-01-028
43. Johnson TV (2009) Review of diesel emissions and control, *International Journal of Engine Research*, 10(5):275–285
44. Johnson TV (2010) Review of Diesel emissions and control, *SAE 2010 World Congress*, 2010-01-0301
45. Chi JN, DaCosta HFM (2005) Modeling and control of a Urea-SCR aftertreatment system, *2005 SAE World Congress* SAE 2005-01-0966
46. Schar CM et al (2006) Control of an SCR catalyst converter system for a mobile heavy-duty application, *IEEE Transactions on Control System Technology*, 14(4):641–652
47. Devarakonda M et al (2009) Model-based estimation and control system development in a Urea-SCR aftertreatment system, *SAE International Journal of Fuels and Lubricants*, 1(1):646–661
48. Seher DHE et al (2003) Control strategy for $NO_x$ - emission reduction with SCR, *Proceedings of the International Truck & Bus Meeting & Exhibition*
49. Devarkonda M et al (2009) Model-based control system design in a urea-SCR aftertreatment system based on $NH_3$ sensor feedback, *International Journal of Automotive Technology*, 10(6):653–662
50. Herman A et al (2009) Model based control of SCR dosing and OBD strategies with feedback from NH3 sensors, *SAE 2009 World Congress*, SAE paper 2009-01-0911
51. Wang DY et al (2009) Ammonia sensor for close-loop SCR control, SAE 2008 World Congress, *SAE International Journal of Passenger Cars- Electronic and Electrical Systems*, 1(1):323–333
52. Hsieh M-F, Wang J (2010) An extended Kalman filter for $NO_x$ sensor ammonia cross-sensitivity elimination in selective catalytic reduction applications, *Proceedings of the 2010 American Control Conference*.
53. Hsieh M-F, Wang J (2012) Adaptive and efficient ammonia storage distribution control for a two-catalyst SCR system, ASME Journal of Dynamic Systems, Measurement and Control, 134(1): 011012.
54. Hsieh M-F (2010) Control of Diesel Engine Urea Selective Catalytic Reduction Systems, Ph.D. Dissertation, The Ohio State University.